Analysis of deformation mechanisms operating under fatigue and dwell-fatigue loadings in an α/β titanium alloy

C. Lavogiez, S. Hémery, P. Villechaise

Analysis of deformation mechanisms operating under fatigue and dwell-fatigue loadings in an α/β titanium alloy

C. Lavogiez[1], S. Hémery[1,*], P. Villechaise[1]

[1] Institut Pprime, CNRS-ENSMA, Université de Poitiers, UPR CNRS 3346, Physics and Mechanics of Materials Departement, ENSMA – Téléport 2, 1 avenue Clément Ader, BP 40109, 86961 Futuroscope Chasseneuil Cedex, France

[*] corresponding author : samuel.hemery@ensma.fr

Abstract

This paper investigates the deformation processes operating in α grains of Ti-6Al-4V submitted to fatigue and dwell-fatigue loadings at room temperature. With this aim, mechanical tests were interrupted after a given number of cycles or cumulated plastic strain. Slip traces analysis combined with electron back-scattered diffraction enabled to evidence the operation of <a> and <c+a> slip, twinning and interface sliding. The main parameters controlling their activity were analyzed, in particular regarding the crystallographic orientation and the load hold duration. Based on this statistically sound investigation, the differences between fatigue and dwell-fatigue behaviors are finally discussed.

Keywords: Titanium alloys, fatigue, dwell-fatigue, slip, twinning

1. Introduction

Titanium alloys are extensively employed in the aerospace industry due to their low density, excellent corrosion resistance and high fatigue strength [1]. They are widely used in gas turbine engines where components such as disks and blades are submitted to complex loading regimes. In particular, the cyclic loadings include a long period at high mean stress during the take-off stage of a flight. In-service failure of components has motivated extensive investigations of the impact of the dwell period on the fatigue performance of near-α and α+β titanium alloys [2,3]. The early laboratory experiments highlighted a reduction in the number of cycles to failure with the introduction of a hold time at maximum stress [4–7]. This dwell-fatigue life debit, also denoted as the cold dwell effect since it stands for temperatures lower than 300°C, has been an important research interest over the past decades. Although the ability of titanium and its alloys to creep at low temperature has been identified as a playing a key role [8], it is not completely understood yet.

Many efforts were firstly put into the identification of crack initiation processes. Early fractographic analyses of crack initiation sites revealed the presence of subsurface quasi-cleavage facets with a basal or near-basal orientation [8,6,9]. The authors proposed a modified version of the

Stroh model to explain the formation of these facets [6]. According to this model, facet formation occurs in a specific microstructural configuration composed of a soft grain where an extensive slip activity occurs and eventually induce dislocation pile-ups at the interface with an adjacent hard grain. The hard grain is poorly oriented for slip along the **<a>** direction due to a basal plane perpendicular to the principal stress direction. Slip modes involving **<a>** directions being the soft slip modes of the α phase in titanium alloys [10–13], the accommodation of the high stress magnitude is difficult. The critical combination of shear stress and tensile stress normal to the basal plane, which is required for facet formation, is reached due to the presence of the stress concentrations induced by dislocation pile-ups [14,15]. The rate sensitive character of plastic deformation was later accounted for using crystal plasticity simulations. The load shedding process from the soft grain onto the hard grain was first simulated by Hasija and coworker [16]. The mean stress in the hard grain is increased with the introduction of a hold time at maximum stress and, in turn, leads to crack initiation. Further simulation works followed to assess the influence of microstructural features [17–23] and testing conditions [24] on this process. Based on these results, crack nucleation was then simulated to predict the dwell fatigue life of titanium alloys [25–29].

The aforementioned models involve crack initiation of grains with their **c**-axis within 15° deviation from the loading axis, in which slip activation is difficult. Nevertheless, several deformation mechanisms were reported to operate in such crystallographic orientations. Recent studies evidenced the occurrence of basal slip in α grains with a declination angle (i.e. the angle between the **c**-axis and the loading direction) as low as 10° under monotonic tension [13], but also the occurrence of twinning and **<c+a>** pyramidal slip in α grains with a declination angle lower than 10° under cyclic loadings [30]. In addition, declination angles as high as 45° were reported from experimental characterizations of the crystallographic orientation at dwell-fatigue initiation facets [31–35]. Owing to the restricted amount of information available regarding the deformation processes operating under cyclic loadings [36,37], the deformation mechanisms associated with dwell-fatigue crack initiation are still unclear.

In contrast, a general agreement is emerging about fatigue crack initiation. The formation of initiation facets is triggered by basal slip activity combined with a high normal stress [36,38]. This distinct mechanism is also accompanied by a surface crack initiation in the low cycle fatigue regime, while sub-surface initiation was reported under dwell-fatigue loadings with a similar peak stress [34]. The macroscopic response also reveals that a higher cumulated plastic strain is sustained under dwell-fatigue loadings than under fatigue loadings [3,4,6,39]. These considerations suggest significant differences in the deformation behavior of titanium alloys depending on the load hold duration. This is confirmed by the different evolutions of deformation patterns over time between monotonic tension, fatigue and dwell-fatigue loadings obtained via strain mapping [40]. These deformation patterns are closely linked to slip system activation and slip localization that depend on the crystallographic orientation and microstructure [41].

In order to elucidate the differences in deformation behavior between fatigue and dwell-fatigue loadings, an analysis of the operating deformation processes in Ti-6Al-4V was performed with different load hold durations to scan testing conditions ranging from fatigue to creep. An extensive characterization of active deformation mechanisms using slip traces analysis combined with electron-back-scattered diffraction is presented in this article based on interrupted tests. The operation of deformation systems is analyzed considering the local crystallographic orientation, the number of cycles, the load hold duration and the cumulated plastic strain. A discussion of its relation with the cyclic deformation behavior and how it may affect crack initiation and growth is provided.

2. Experimental

2.1 Material and specimens

The material in this study was a Ti-6Al-4V alloy with a bi-modal microstructure composed of primary equiaxed α grains and colonies of secondary α lamellas embedded in a β matrix. A micrograph showing the microstructure of the material is presented in figure 1a. The average diameter of the equiaxed α grains and the associated surface fraction are 13 µm and 36 %. The distribution of crystallographic orientations relative to the loading direction is presented on the inverse pole figure shown in figure 1b. The maximum intensity is about 1.7 times random, which indicates a weak texture.

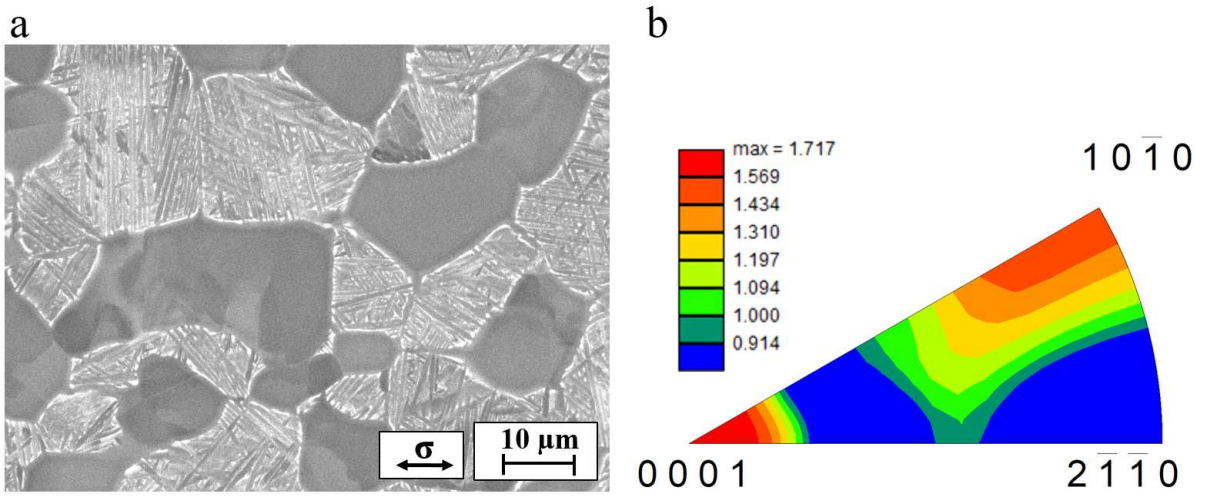

Figure 1 - a) SEM micrograph showing the microstructure and b) inverse pole figure plot of the orientation distribution function with respect to the tensile direction showing the texture

Flat dog bone specimens were machined using electrical discharge machining. The gage length is 10 mm, the gage width is 2 mm and specimens are 1 mm thick. For further information about the specimen geometry, the reader is referred to [13]. In order to enable slip traces detection as well as electron back-scattered diffraction (EBSD) characterization, the samples were first ground finishing with grade 4000 SiC paper. Then, the samples were polished using a 9 µm diamond suspension. A final polishing step was applied using a 9:1 solution of colloidal silica suspension with a mean particle size of 0.04 µm to H_2O_2.

2.2 Mechanical testing

An in situ tensile test was first performed in a JEOL 6100 scanning electron microscope (SEM). The aim was to characterize slip activation under monotonic tension. This served as a basis to design cyclic testing conditions. The specimen was loaded using a DEBEN 5 kN tensile testing machine with a constant displacement rate of 0.02 mm / min. After reaching a targeted stress value, the displacement was stopped to allow the acquisition of micrographs in the region of interest for a total area of 230 x 540 µm². From the detection of the first slip trace, stops were made every 10 MPa until reaching a plastic strain of 0.2 %. The strain in the gage length was continuously recorded using a strain gage.

In order to study the operating deformation processes in relation with the microstructure and the loading conditions such as the duration of the load hold, cyclic tests were performed under controlled load. A trapezoidal loading waveform was applied to allow the introduction of a hold time at maximum stress. The duration of the load hold is denoted as t_{hold} in the following. A 1 s linear rise and fall was incorporated between minimum and maximum loads. The hold period at minimum stress was 1 s. The load ratio was taken equal to 0.1. Two sets of experiments were performed with different peak stress magnitudes which were defined using the results of the in situ tensile test and relatively to the 0.2 % proof stress of the material. In the following, the different levels of applied stress will be referred to as low stress (LS) and high stress (HS). The 0.2 % proof stress ($\sigma_{0.2\ cyclic}$) is 966 MPa. This

value was determined using a dedicated tensile test with an applied strain rate of 10^{-2} s^{-1} in order to reproduce the 1 s loading used for cyclic tests. To characterize the evolution of operating deformation processes during cycling, the tests were interrupted at targeted cumulated plastic strain values or number of cycles.

Prior studies showed that the deformation patterns are established early in the loading history [40]. The evolution of the operating deformation processes was thus monitored during the first cycles of the fatigue and dwell-fatigue LS tests using SEM observations. The number of cycles performed before each interruption is presented in table 1 along with the associated cumulated plastic strain. With the exception of the first stop, which was made after one cycle, interruptions were performed at similar cumulated plastic strains. The HS tests were carried out to investigate the influence of the hold duration at maximum applied stress. The hold time at maximum stress was varied to scan loading conditions from fatigue (t_{hold} = 1 s) to creep (t_{hold} = 425 s) while considering dwell-fatigue loadings (t_{hold} = 30 s, 60 s or 120 s). For the creep test, the load was held until the targeted plastic strain was reached. Tests were interrupted at a cumulated plastic strain of 2.5%. The active deformation processes were then investigated.

Fatigue LS		Dwell-fatigue LS	
N cycles	Plastic strain	N cycles	Plastic strain
1	0.20×10^{-3}		
60	1.01×10^{-3}	1	1.01×10^{-3}
279	3.01×10^{-3}	4	2.87×10^{-3}
1351	9.98×10^{-3}	65	1.02×10^{-2}

Table 1 – Number of cycles and cumulated plastic strain at interruptions of the LS fatigue and dwell-fatigue tests

2.3 Characterization of active deformation processes

The active deformation processes were mainly studied using SEM observations of the surface of the deformed specimens. The SEM micrographs, which were employed for microstructural characterization and slip traces analysis, were acquired using a JEOL 6100 SEM and a JEOL 7000F field emission gun – SEM. The EBSD technique was employed in order to characterize the local crystallographic orientation using Hikari and Digiview detectors provided by EDAX and mounted on a JEOL 6100 SEM and a JEOL 7000F field emission gun – SEM. The step was adjusted to the length-scale of the investigated elements.

2.3.1 Slip trace analysis

The active slip systems were investigated using slip traces analysis. Only equiaxed α grains were considered as early deformation processes and fatigue crack initiation occur in these microstructural elements. Several regions were studied for each specimen in order to analyze the operating deformation systems with a statistical significance. These regions were carefully selected to in order to exhibit similar and weak textures. This procedure enables to consider the entire crystallographic orientation domain while avoiding texture related bias in the analyses. All the slip systems detected as active in these regions were considered. Per testing condition, 399 ± 146 grains were investigated leading to 492 ± 90 slip systems analyzed at the final loading steps among which 299 ± 50 were successfully identified.

Slip traces observed on SEM micrographs were compared with the theoretical traces of the prismatic, basal and 1st order pyramidal planes calculated using EBSD data. The experimental traces were considered matching theoretical ones if the misorientation between the traces is lower than 5°. If multiple theoretical traces correspond to an experimental slip trace within the 5° angular tolerance, the investigated case was ruled out of the analysis. As slip traces analysis only provides information about the slip planes, the slip direction of the active slip system had to be inferred. Regarding prismatic slip, each slip plane is associated with one slip direction. In this case, the determination of the active slip system is straightforward. For basal slip, the slip system with the highest Schmid factor was assumed

to be active. The situation is more complex for slip on 1st order pyramidal planes as it may occur along either **<a>** or **<c+a>** directions. As the critical resolved shear stress (CRSS) values differ significantly, it was used to determine whether **<a>** or **<c+a>** slip was associated with an experimentally observed pyramidal slip trace. The approach introduced by Lunt et al. was applied [42]. A normalized Schmid factor is calculated by dividing the Schmid factor using a relative CRSS value of 1.3 for pyramidal slip along the **<a>** direction and 1.6 for pyramidal slip along the **<c+a>** direction. The values of the CRSS ratios were taken from the work of Bridier and coworker [43]. The slip system leading to the highest normalized Schmid factor was considered to be active. An example of a slip trace analysis is shown in figure 2.

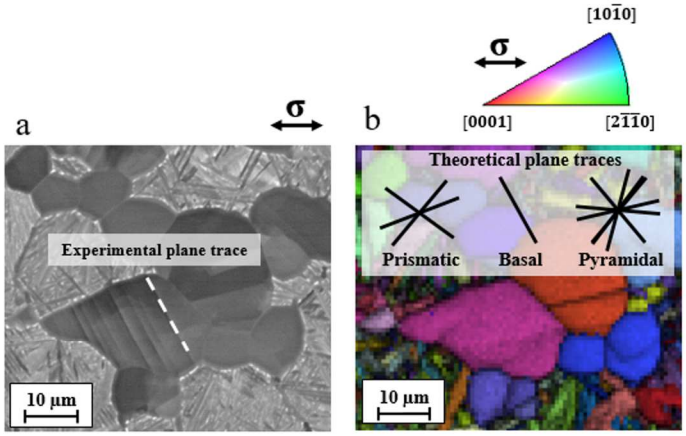

c

Plane	Direction	Schmid factor
(0001)	[11$\bar{2}$0]	0.402
(0001)	[1$\bar{2}$10]	0.033
(0001)	[$\bar{2}$110]	0.435

Figure 2 : Example of slip trace analysis involving the following steps a) detection of slip traces on a SEM micrograph, b) comparison with the theoretical plane traces calculated using EBSD data and c) identification of the active slip system considering the magnitude of the Schmid factors. According to this analysis the slip trace corresponds to a basal slip system with a Schmid factor of 0.435.

The Schmid factor was also used for the analysis of the operating deformation mechanisms. In polycrystalline materials, a heterogeneous stress field results from the elastic and plastic anisotropies of α titanium [44]. However, this geometric parameter can be considered as a semi-quantitative indicator of the resolved shear stress level on the associated slip system. Indeed, Bridier et al. showed that it is good indicator for slip activation when statistically significant data is considered [13].

2.3.2 Detection of twins

Prior work evidenced the occurrence of twinning in Ti-6Al-4V submitted to cyclic loadings [30]. Owing to the small size of these twins, a very small EBSD step had to be applied for a reliable detection. A 70 nm step was presently used. In order to maintain a statistical significance of the analysis, twinning was characterized only on the fatigue and 120 s dwell-fatigue HS tested specimens. The active twinning system and the associated Schmid factor are determined using the crystallographic orientations of twins and parent grains. An example of such analysis is shown in [30].

The occurrence of twinning was systematically found associated with an incoming slip band. The geometric alignment between incoming and outgoing deformation systems was investigated using the *m'* parameter introduced by Luster and Morris [45]. The alignment is evaluated on a scale from 0

to 1. 1 corresponds to a perfect alignment between both systems. The equation used to calculate *m'* values is given in equation 1.

$$m' = \cos \kappa \times \cos \psi \quad (1)$$

With κ the angle between the normals to the slip and twin planes and ψ the angle between the slip and twin directions.

3. Results

3.1 Mechanical response

As a preliminary study, slip activation was characterized using an in situ tensile test carried out inside a SEM. Slip activity in the region of interest was monitored up to a 0.2 % plastic strain offset, which was reached at 772 MPa ($\sigma_{0.2\ in\ situ}$). This value is somewhat lower than $\sigma_{0.2\ cyclic}$ due to the difference in loading rate. Basal slip was firstly detected at the 650 MPa step. This applied stress corresponds to 84 % of $\sigma_{0.2\ in\ situ}$. Prismatic slip activation was then detected at a stress level of 710 MPa, which corresponds to 92 % of $\sigma_{0.2\ in\ situ}$. The detection of basal slip before prismatic slip is consistent with previous observations [46]. For more details about the relative activity of the different slip modes as a function of the applied stress, the readers are referred to prior studies [46,47]. Assuming a global stress state, an apparent CRSS was estimated using the Schmid factor of the identified slip system and the applied stress at slip trace appearance. A recent study on Ti-6Al-4V revealed a very limited bias in CRSS estimation based on this assumption which neglects elastic anisotropy and grains interactions [44]. The average values are 309 MPa for basal slip and 333 MPa for prismatic slip. These values, which are in very good agreement with those reported in the literature for a similar α grain size [48], confirm the difference in applied stress required for the activation of basal and prismatic slip. The sensitivity of the dwell-fatigue life debit with respect to the applied peak stress might be related to this characteristic. In order to investigate the relation between the active deformation systems and the deformation behavior under cyclic loadings, the peak stress of the LS and HS tests were set at 869 MPa (i.e. 0.90 x $\sigma_{0.2\ cyclic}$) and 908 MPa (i.e. 0.94 x $\sigma_{0.2\ cyclic}$) respectively. This normalization allows to overcome the difference in loading rate between the in situ SEM and cyclic tests. As a result, only basal slip is expected at the first loading segment of the LS tests while both basal and prismatic slip are expected at the first loading segment of the HS test.

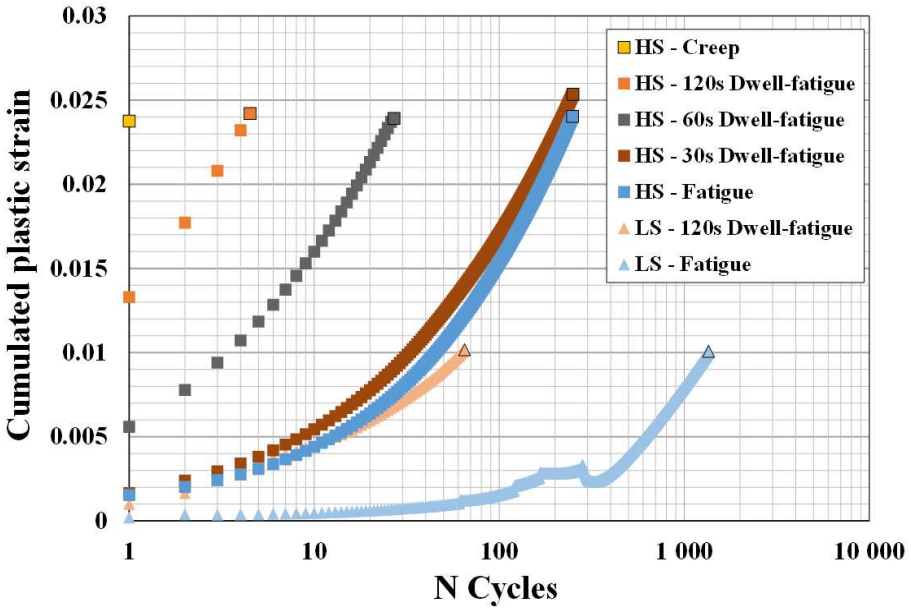

Figure 3 : Cumulated plastic strain with respect to the number of cycles for the LS and HS tests showing a significant strain accumulation during load holds

The evolution of the cumulated plastic strain as a function of the number of cycles for the LS and HS tests is presented in figure 3. First considering the HS tests, the experiments were successfully stopped at a cumulated plastic strain of 2.5%. The number of cycles needed to reach the targeted plastic strain decreases as the hold time at maximum stress is increased. The reduction in number of cycles seems weak between the fatigue and the 30 s dwell-fatigue tests but it is significant for the hold periods of 60 s and 120 s. For instance, 250 fatigue cycles were achieved to reach the targeted plastic strain while only 5 were needed with a 120 s load hold. This feature reveals the occurrence of room-temperature creep during the load hold at maximum stress. The targeted plastic strain was indeed reached after 425 s for the creep test. This value does not show a rapider strain accumulation for dwell-fatigue than for creep as expected from literature data [49]. This may result from the slight variability in the mechanical response from one specimen to another. Within this batch of experiments, the aim is to extract global trends rather than a direct comparison between two testing conditions with a slight difference in load hold duration (typically by a factor 2). Such bias is not expected for the LS tests due to the increase in load hold duration by a factor 120. Regarding the LS tests, a reduction in number of cycles required to achieve similar plastic strain levels is also observed with the increase in the load hold duration. For example, 60 fatigue cycles were required to reach the same plastic strain as 1 dwell-fatigue cycle including a 120 s load hold. Similarly, 65 dwell-fatigue cycles with a 120 s load hold were needed to reach 1 % cumulated plastic strain while 1351 fatigue cycles were needed.

3.2 Basal and prismatic slip

Basal and prismatic slip systems being soft deformation modes of the α phase of titanium alloys, they account for the majority of the active deformation system. Any significant difference in the deformation behavior depending on the load hold duration, such as evidenced in the previous paragraphs, should thus result from differences in the basal and prismatic slip activity. It was first analyzed with respect to the number of cycles. A comparison at similar cumulated plastic strain was also performed.

3.2.1 Slip activity after 1 cycle

The crystallographic orientation relative to the loading direction of α grains with basal or prismatic slip traces after 1 LS fatigue cycle is shown in figure 4a. Two distinct populations can be distinguished. α grains with basal or prismatic slip traces correspond to restricted orientation domains that do not overlap. Figure 4c and 4d display the Schmid factor distributions. The reported fractions correspond to the number of slip occurrences within a given Schmid factor bin divided by the number of α grains with a maximum Schmid factor within the same bin. Prismatic slip occurred for Schmid factors of at least 0.35 while basal slip occurred for Schmid factors as low as 0.25. Considering that the Schmid factor is indicative of the magnitude of resolved shear stress on a given slip system, these values are consistent with the lower CRSS for basal slip than for prismatic slip. The maximum fractions, which are about 0.18 and 0.09 for basal and prismatic slip, reveal that all slip systems with a high Schmid factor were not associated with slip traces. According to these observations, basal slip is dominant for such test conditions. In contrast, prismatic slip activity is sparse and mainly associated with very high Schmid factors. No prismatic slip was expected from the in situ tensile test. However, the slip traces analysis was carried out after the end of a complete cycle. Thus, it includes the loading step plus the 1 s load hold and unloading steps. The plastic strain cumulated during the loading and hold segments are 0.7×10^{-4} and 0.9×10^{-4} respectively. The similar plastic strain levels cumulated at each step suggest that prismatic slip activation may have occurred during the 1 s load hold.

The crystallographic orientation of α grains with basal or prismatic slip traces after the first 120 s LS dwell-fatigue cycle is shown in figure 4b. A balanced representation of basal and prismatic slip systems is observed. Different orientation domains are noticed depending on the slip

mode considered. However, overlap occurs for orientations corresponding to low Schmid factor values for both slip modes according to the Schmid factor iso-contours reported in [13]. Figure 4 c and d display the Schmid factor distributions. Basal and prismatic slip proceed for Schmid factors of at least 0.2 but most of slip traces were observed for Schmid factors higher than 0.3. On average, basal slip was observed for lower Schmid factors than prismatic slip. The maximum fractions, which are about 0.5 and 0.28 for basal and prismatic slip, also reveal that slip systems with a high Schmid factor were not systematically associated with slip traces.

The comparison of the deformation behavior after the first fatigue cycle and the first 120 s dwell-fatigue cycle reveals significant differences. Due to the strain accumulation occurring during the hold time at maximum stress, the plastic strain after the first 120 s dwell-fatigue cycle (0.3 %) is higher than after 1 fatigue cycle (0.1 %). According to figures 4a and 4b, this is accompanied by a higher number of α grains with slip traces. In addition, orientation domains are extended for both basal and prismatic slip if a 120 s load hold is applied. The comparison of Schmid factor distributions reveals an increase in the fraction of α grains with basal or prismatic slip traces for any Schmid factor bin with the increased load hold duration. For instance, 50 % of α grains where a basal slip system is associated with a Schmid factor higher than 0.45 exhibited basal slip traces after the first 120 s dwell-fatigue cycles versus only 12 % after the first fatigue cycle. Similarly, 28 % of α grains with a prismatic slip system associated with a Schmid factor higher than 0.45 exhibited prismatic slip traces after the first 120 s dwell-fatigue cycle versus only 9 % after the first fatigue cycle. The Schmid factor range associated with slip activity is also extended towards lower values with the increase in load hold duration.

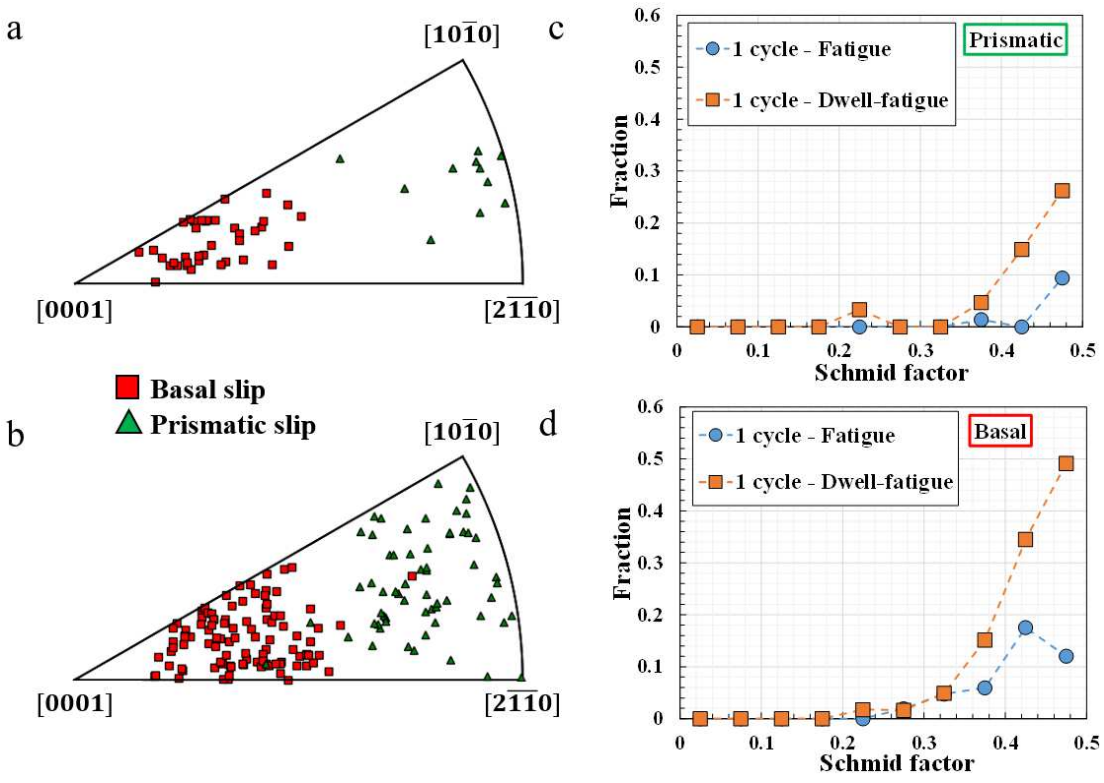

Figure 4: Crystallographic orientation of α grains with basal and prismatic slip traces after the first cycle of a) fatigue and b) 120 s dwell-fatigue LS tests. The orientations are relative to the loading direction. Schmid factor distributions for c) prismatic slip and d) basal slip showing different slip activities

3.2.2. Slip activity at similar plastic strain (1 dwell-fatigue cycle – 60 fatigue cycles)

Slip activities were found to differ significantly depending on the load hold duration of the first cycle. However, this is also accompanied by different cumulated plastic strain values. In order to

make up for the introduced bias, slip activity was then analyzed for a similar cumulated plastic strain. This approach, which implies a different number of cycles, allows to highlight the effect of the cycling process.

The same cumulated plastic strain as reached after the first 120 s dwell-fatigue cycle was obtained after 60 fatigue cycles. The crystallographic orientation of α grains with basal or prismatic slip traces after 60 fatigue cycles is shown in figure 5a. The comparison with the plot of figure 4a reveals that numerous α grains without slip traces after the first cycle exhibit slip traces after the 60^{th} cycle. Schmid factor distributions shown in figure 4 and 5 demonstrates that slip systems with low Schmid factors are more likely to be active after 60 cycles. For instance, slip systems with Schmid factors as low as 0.2 are found active after 60 cycles while this was not observed after 1 cycle. In addition, the fraction is increased after 60 cycles for a given Schmid factor bin. 38 % of the α grains present prismatic slip traces after 60 cycles versus only 10 % after the first cycle for the 0.45 – 0.5 interval.

The comparison of slip activities after the first 120 s dwell-fatigue cycle and after 60 fatigue cycles reveals interesting features. According to figures 5a and 6a, a similar amount of α grains with basal or prismatic slip traces is noticed for both loading conditions. The ratio of the number of active slip systems detected and the number of α grains in the region of interest, which is 0.30 for 60 fatigue cycles and 0.27 for one 120 s dwell-fatigue cycle, is similar as well. The Schmid factor distributions shown in Figure 5 and Figure 6 for a cumulated plastic strain of 0.001 are also very similar. For instance, slip occurs for Schmid factors higher than 0.2 under both fatigue and 120 s dwell-fatigue loadings. In the early loading history, slip activity is thus significantly different considering a similar number of cycles while no difference could be detected at a similar cumulated plastic strain. In the following, a comparison of slip activity at similar but higher cumulated plastic strain levels was carried out in order to evidence any noticeable influence of the load hold duration.

3.2.3. Slip activity at similar plastic strain

To investigate if the previously suggested equivalence is maintained with an increasing cumulated plastic strain, the same approach was applied after 4 and 65 dwell-fatigue cycles including a 120 s load hold. Cumulated plastic strains of 0.3 % and 1 % were reached. They correspond to 279 and 1351 fatigue cycles. The crystallographic orientation of α grains with basal or prismatic slip traces are presented on figure 5 for the fatigue test. The full symbols corresponds to α grains where newly activated slip systems were noticed, while empty symbols indicate that slip activity had already been noticed at previous steps. As the cumulated plastic strain or the number of cycles increases, prismatic and basal slip activation is observed. However, the number of newly activated slip systems decreases as shown in figure 5b and 5c. The Schmid factor distribution at each step is shown in figure 5d and 5e for basal and prismatic slip systems. These distributions include the active slip systems noticed at previous steps. The fraction for prismatic slip with a Schmid factor between 0.35 and 0.4 is 0.08 at a cumulated plastic strain of 0.001 while it is 0.22 at a cumulated plastic strain of 0.01. Similarly, the fraction for basal slip increases from 0.1 to 0.24. The fractions corresponding to Schmid factors higher than 0.45 are also observed to increase for both slip system. It increases from 0.38 for prismatic slip at a plastic strain of 0.001 to 0.52 at a plastic strain of 0.01. Regarding basal slip, this fraction increases from 0.38 to 0.48. This illustrates an increasing number of active slip systems with an increasing cumulated plastic strain and / or number of cycles. However, the previous values reveal that newly activated slip systems are mainly associated with low Schmid factors.

Regarding the 120 s dwell-fatigue test, the orientation of α grains where newly activated slip systems were observed is reported in figure 6 a-c for the same cumulated plastic strains as the fatigue test. The evolution of the crystallographic orientations for basal and prismatic slip shows similarities with the fatigue test. Although the number of α grains with slip traces increases, the number of α grains with newly activated slip systems decreases as the cumulated plastic strain (or the number of

cycles) increases. Since full symbols get closer to the [0001] pole of the inverse pole figure plots for increasing cumulated plastic strain or number of cycles, basal slip operates in α grains with lower declination angles. This feature was not so clear for the fatigue test. The Schmid factor distributions as a function of the number of cycles / cumulated plastic strain are plotted on figure 6d and 6e for prismatic and basal slip. For Schmid factors higher than 0.2, the fractions increase with the cumulated plastic strain. A similar feature was noticed for the fatigue test.

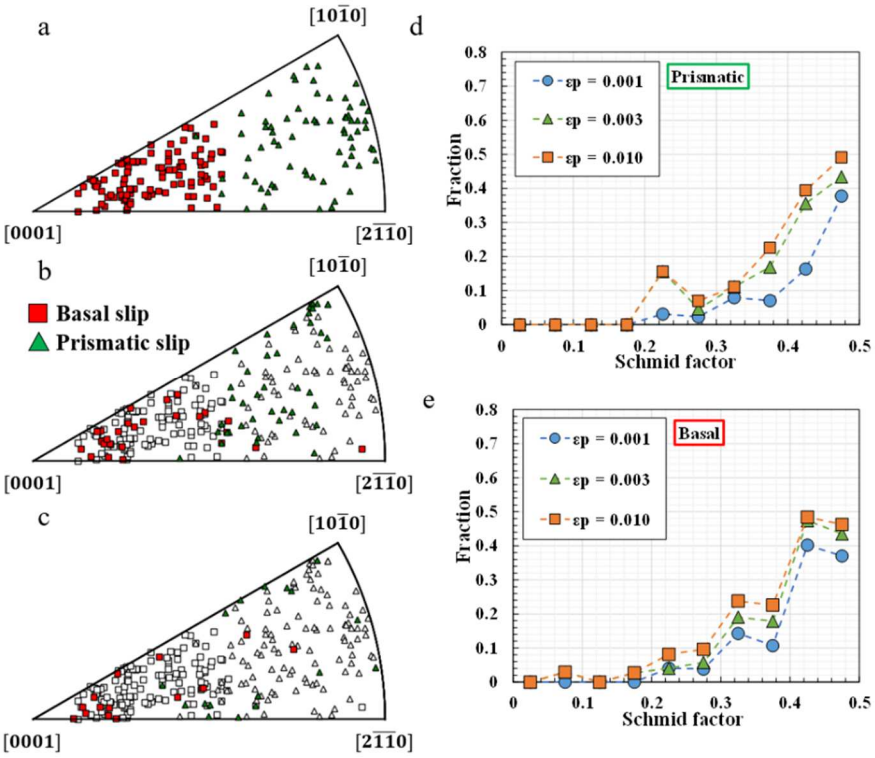

Figure 5: Crystallographic orientation of α grains showing basal and prismatic slip traces at cumulated plastic strains of a) 0.001 b) 0.003 and c) 0.010 for the LS fatigue test. The orientation is relative to the loading direction. Full symbols indicate newly activated slip systems and empty symbols indicate previously noticed slip activity. Schmid factor distributions for d) prismatic slip and e) basal slip.

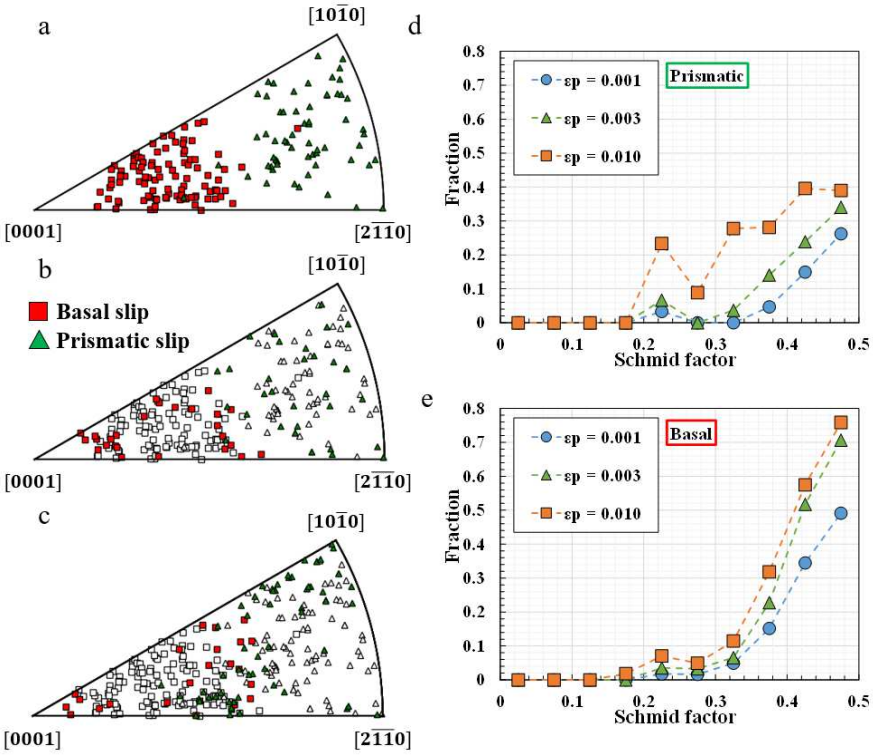

Figure 6: Crystallographic orientation of α grains showing basal and prismatic slip traces at cumulated plastic strains of a) 0.001 b) 0.003 and c) 0.010 for the LS 120 s dwell-fatigue test. The orientation is relative to the loading direction. Full symbols indicate newly activated slip systems and empty symbols indicate previously noticed slip activity. Schmid factor distributions for d) prismatic slip and e) basal slip.

The total number of basal and prismatic active slip systems was divided by the total number of α grains contained in the regions of interest. The resulting fractions are reported in figure 7 with respect to the cumulated plastic strain for the fatigue and 120 s dwell-fatigue LS tests. Although the fractions are similar up to a cumulated plastic strain of 3 x 10^{-3}, it is higher for the dwell-fatigue test beyond this value. More slip systems are thus operating and contribute to the deformation at high plastic strains if a load hold is applied.

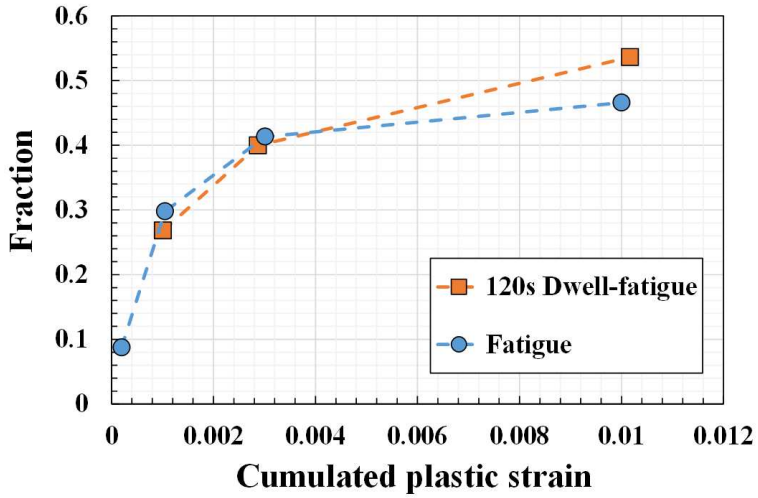

Figure 7: Fraction calculated as the total number of basal and prismatic active slip systems divided by the number of α grains in the regions of interest for the fatigue and 120 s dwell-fatigue LS tests plotted with respect to the cumulated plastic strain.

3.2.4 *Influence of load hold duration on slip activity*

In order to confirm the previous findings at a different peak stress while investigating the effect of the load hold duration on slip activity, the HS set of tests was carried out. Subsequent analyses of basal and prismatic slip activity are presented in the following.

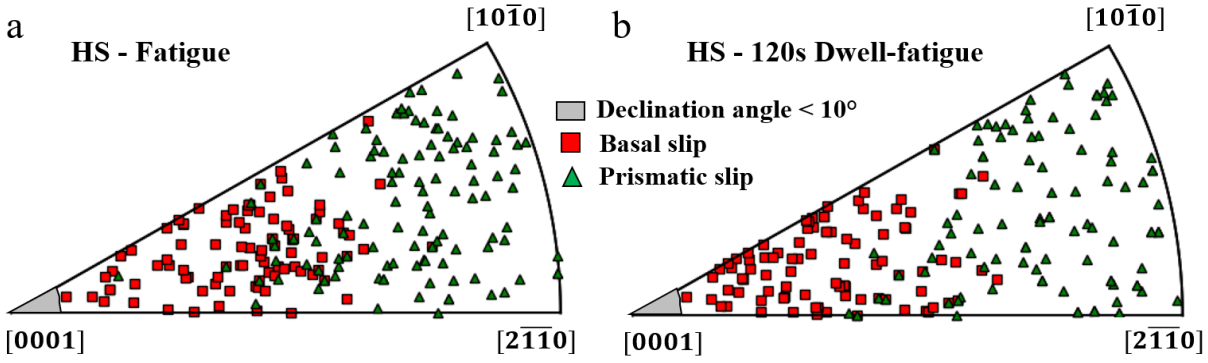

Figure 8: Crystallographic orientation of α grains showing basal and prismatic slip traces at a cumulated plastic strain of 0.025 for the a) fatigue and b) 120 s dwell-fatigue HS tests. The orientation is relative to the loading direction.

The crystallographic orientation of α grains where prismatic or basal slip traces were noticed for the HS fatigue test and the HS 120 s dwell-fatigue test is shown in figure 8. In agreement with observations carried out for the LS tests, the crystallographic orientations associated with the occurrence of basal or prismatic slip are significantly different. However, a substantial overlap is observed. Neither basal nor prismatic slip traces were noticed on α grains with a declination angle lower than 10 °.

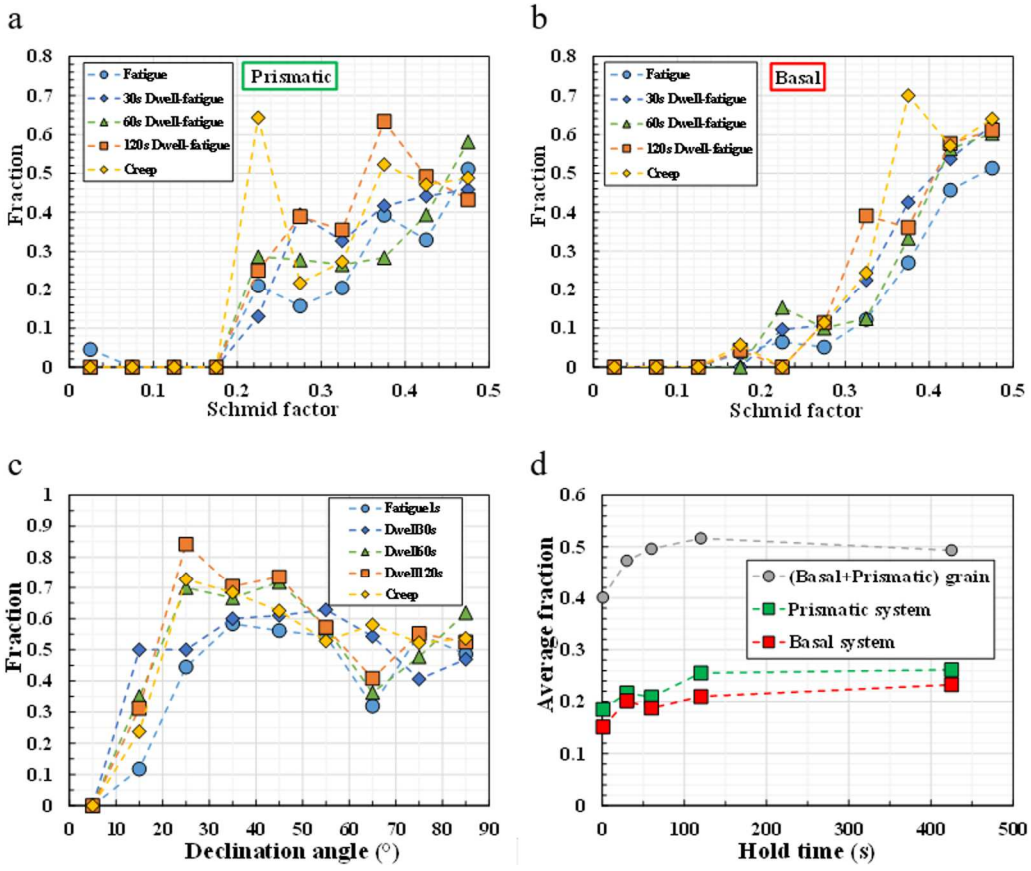

Figure 9: Schmid factor distributions for a) prismatic slip and b) basal slip, c) fraction of α grains with basal or prismatic slip traces with respect to the declination angle and d) average of the fractions displayed in figures 8a (basal system), 8b (prismatic system) and 8c ((basal+prismatic) grain) for each load hold condition showing i. an increase in the number of active basal and prismatic slip systems and ii. an increase in the number of α grains with basal or prismatic slip activity with higher load hold duration but similar cumulated plastic strains for the fatigue, dwell fatigue and creep HS tests.

The Schmid factor distributions for basal and prismatic slip are presented in figure 9a and 9b for the HS tests. Basal and prismatic slip activities are noticed for Schmid factors ranging from 0.2 to 0.5. For low Schmid factor values (<0.15 – 0.2), the resolved shear stress seems insufficient to activate basal or prismatic slip. Although very similar distributions are obtained for any load hold duration, the fatigue test defines the lower bound of the fractions for both prismatic and basal slip. In addition, the higher bounds are defined by the creep or 120 s dwell-fatigue tests, which include high load hold durations. An increased hold time thus leads to higher fractions. In order to confirm this finding, the average of the fractions presented in figure 9a and 9b are shown as a function of the load hold duration in figure 9d. These values represent the average number of active basal or prismatic slip system per α grain for a material with a homogeneous Schmid factor distribution. The resulting values are increasing with the load hold durations. For instance, a value of 0.15 is obtained for basal slip under fatigue loading while the values are 0.21 for the 120 s dwell-fatigue loading and 0.23 for the creep loading. Regarding prismatic slip, the value is 0.19 under fatigue loading while the values are 0.26 for the 120 s dwell-fatigue or creep loadings. More slip systems thus contributes to the deformation as applied load hold durations are increased.

As several active slip systems were often detected in a single α grain for HS tests, these values do not reflect the fraction of α grains deforming via basal or prismatic slip. The ratio of the number of α grains with basal or prismatic slip traces to the number of α grains in a given declination angle interval is shown in figure 9c with 10° bins. Although very similar distributions are obtained for any load hold duration, the fatigue test mostly defines the lower bound of the fractions. In addition, the higher bounds are mainly defined by the creep or 120 s dwell-fatigue tests, which include high load hold durations. An increased hold time thus seems to lead to higher values. In order to confirm this finding, the fractions were averaged for each loading condition to represent the fraction of α grains with basal or prismatic slip traces in a material with a homogeneous declination angle distribution. The resulting values, which are presented in figure 9d, increase with the load hold duration. Soft slip modes are thus active in a higher number of α grains with an increasing load hold duration.

3.3 Other deformation modes: boundary sliding, pyramidal slip and twinning

Although basal and prismatic slip were studied with statistical significance, other deformation modes, such as grain boundary sliding, pyramidal slip and twinning, were more rarely observed and their identification required a more in-depth characterization approach. As a consequence, a thorough analysis is presented in the following paragraphs for the fatigue and 120 s dwell fatigue HS tests.

3.3.1 Slip stimulated grain boundary sliding

Examination of the surface of the deformed specimens revealed the presence of grain boundary ledges such as described in [50], which indicates the occurrence of grain boundary sliding. It was mainly observed along interfaces between highly and slightly deformed microstructural elements. This process seems stimulated by intragranular slip. A typical example is shown on the micrograph presented in figure 10a. Slip traces on the surface of the equiaxed α grain are consistent with prismatic slip activity. These slip traces appear deflected into the interface. The interactions between the prismatic slip bands and the boundary thus seemingly triggered the formation of a grain boundary ledge. This process was noticed multiple times for the HS tests. The crystallographic orientation of the α grains associated with grain boundary sliding is shown on figure 10b for the fatigue and 120 s dwell-

fatigue HS tests. These orientations are similar to those reported in [50] and do not seem affected by the load hold duration. These results consistently support previous findings as they suggest a key role of prismatic slip in stimulating the boundary sliding process.

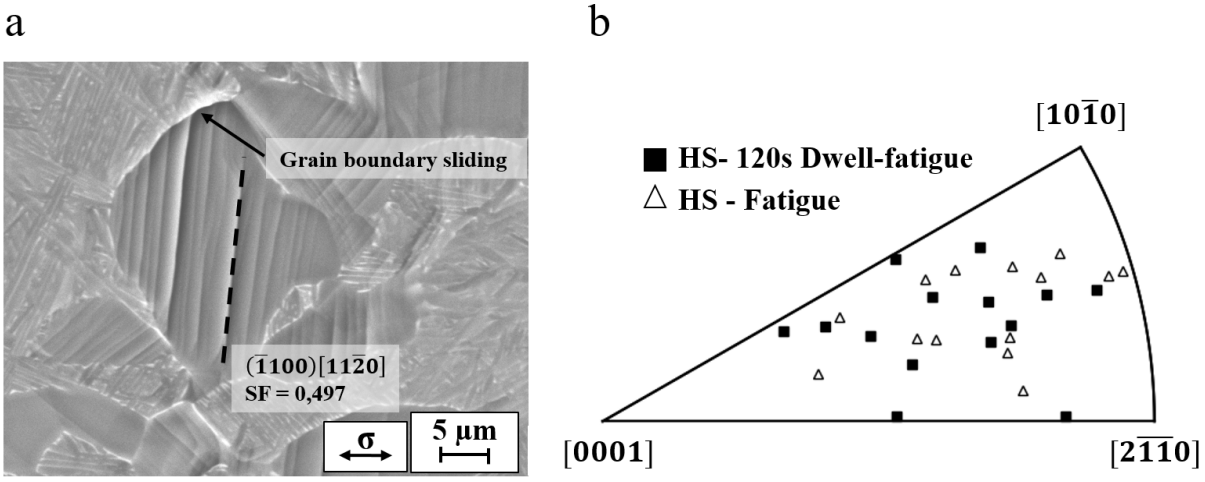

Figure 10: a) SEM micrograph showing the occurrence of prismatic slip stimulated grain boundary sliding and b) crystallographic orientation of α grains showing grain boundary sliding at a cumulated plastic strain of 0.025 for the fatigue and 120 s dwell-fatigue HS tests. The orientations are relative to the loading direction.

3.3.2 Pyramidal slip

Although basal and prismatic slip activity was found dominant in the previous analysis, pyramidal slip traces have been also identified in LS and HS tests. However, the restricted number of occurrences only allowed a statistically significant analysis for the HS tests, which is described in the following. A micrograph showing an α grain (denoted as grain H) with pyramidal slip traces on its surface is presented in figure 11a. The local crystallographic orientation in the same region is given in figure 11b. The analysis of slip traces reveals the operation of two **<c+a>** pyramidal slip systems with maximum Schmid factors of 0.46 and 0.47. The potential operation of **<a>** pyramidal slip was ruled out based on an analysis of the modified Schmid factors. **<c+a>** pyramidal slip traces are generally associated to a high density of evenly spaced slip lines. These fine slip lines suggest a lower displacement carried by each slip band than for basal or prismatic slip bands. As a result, a more homogeneous plastic strain may be expected due to the operation of **<c+a>** slip. Near the interface with the S1 grain, the slip traces continuously extends across the interface. This feature reveals the occurrence of slip transfer. The incoming slip bands, located in S1, correspond to a prismatic slip system with a Schmid factor of 0.45.

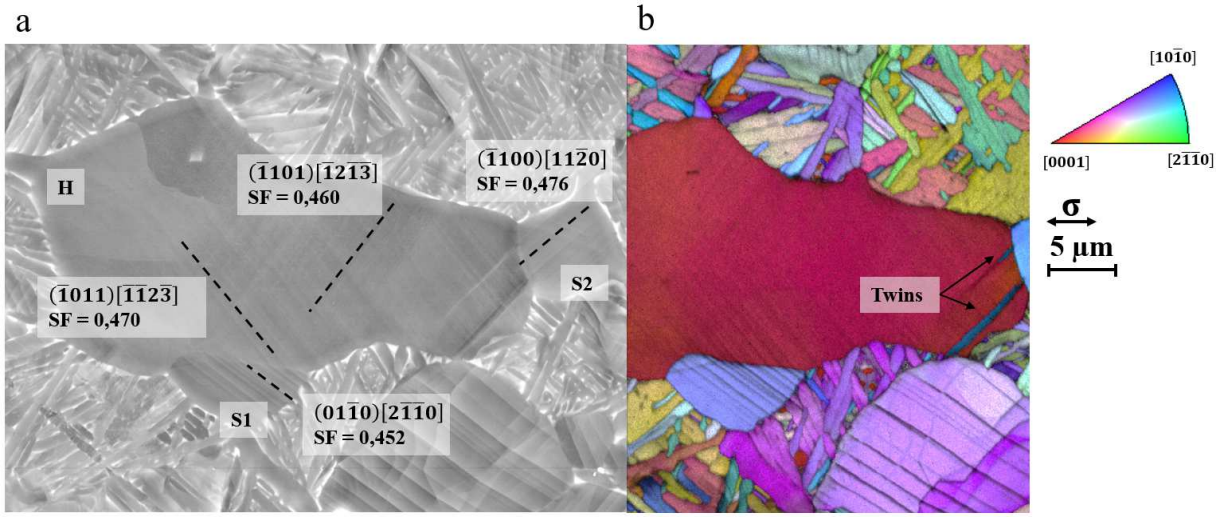

Figure 11: a) SEM micrograph of a hard grain showing <c+a>pyramidal slip traces and twins on the surface of the 120 s dwell-fatigue HS tested specimen at ε_p = 2.5%. b) Corresponding crystallographic orientation map relative to the loading direction.

In order to obtain insights into conditions favoring pyramidal slip, the crystallographic orientation of α grains where pyramidal slip traces were identified is shown in figure 12a and 12b. Two populations, which are consistent with the iso-contours of Schmid factor for 1st order pyramidal slip along the **<c+a>** direction [51], can be distinguished. Although only **<c+a>** slip occurred near the [0001] pole (i.e. for low declination angles), both **<a>** and **<c+a>** slip are likely to be activated for higher declination angles, closer to the prismatic pole. According to the orientation of α grains where **<a>** pyramidal slip traces were noticed, the operation of **<a>** pyramidal slip is also associated with high Schmid factors [51].

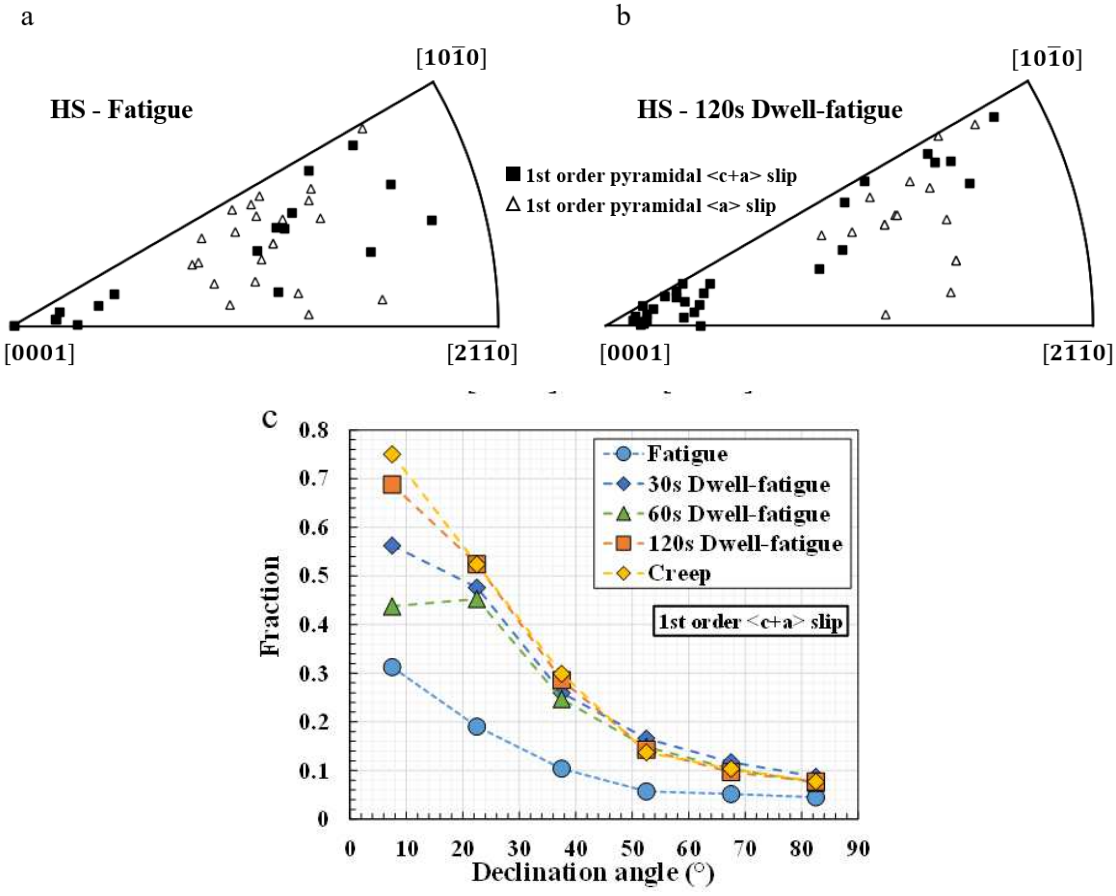

*Figure 12: Crystallographic orientation of α grains showing first order pyramidal slip traces along the <**a**> and <**c+a**> directions at cumulated plastic strains of 0.025 for the a) fatigue and b) 120 s dwell-fatigue HS tests. The orientations are relative to the loading direction. c) Declination angle distribution of <**c+a**> first order pyramidal slip depending on the load hold duration of the HS tests.*

The inverse pole figure plots reveal a higher number of α grains with **<c+a>** pyramidal slip traces near the basal pole for the 120 s dwell-fatigue test than for the fatigue test. In order to dismiss a potential texture related bias, the number of α grains with **<c+a>** pyramidal slip activity for a given range of declination angle was divided by the number of α grains within the same range of declination angle. The resulting fractions are shown in figure 12c. The fractions are close to zero for declination angles higher than ≈ 45°. Below 45°, **<c+a>** pyramidal slip is observed in a significant proportion of α grains. In this range of declination angle, the fractions of the fatigue tested specimen constitute the lower bounds for any declination angle interval. For instance, the fraction of α grains with a declination angle lower than 10° range from 30 % for the fatigue test to more than 75 % for the creep test. Significantly different values are thus obtained depending on the load hold duration. An increased duration of the load hold favors **<c+a>** pyramidal slip activity in α grains with a low declination angle.

3.3.3 $\{10\bar{1}2\}\langle 10\bar{1}1\rangle$ extension twinning

The presence of $\{10\bar{1}2\}\langle 10\bar{1}1\rangle$ twins was noticed on the surface of tested specimens. The operation of $\{10\bar{1}2\}\langle 10\bar{1}1\rangle$ twinning under cyclic loadings was also reported in a previous study [30]. A micrograph showing an α grain (denoted as grain H) containing twins is presented in figure 11a. In this example, the twins seem stimulated by prismatic slip bands with a Schmid factor of 0.48 present in the S2 equiaxed α grain.

The presence of twins was investigated in the fatigue and 120 s dwell-fatigue HS tested specimens. The area of the twins range from 1 µm² to 4 µm². The crystallographic orientation of α grains containing twins is reported in figure 13. The crystallographic orientation of the parent α grains does not seem influenced by the load hold duration. Twins were only noticed in grains with declination angles lower than 20°. Within this orientation domain, twins were identified in 10 α grains among the 39 grains contained in the region of interest of the 120 s dwell-fatigue specimen. In the fatigue tested specimen, 9 α grains containing twins have been identified among the 34 α grains considered. Most of the twins were noticed in α grains with a declination angle lower than 10° while only a few were found beyond 10°. Twins were exclusively detected in α grains where no evidence of basal slip was found. The crystallographic orientation of α grains with basal or prismatic slip activity is also indicated in figure 13. This confirms the different orientation domains associated with these deformation modes. As twinning was systematically observed to be stimulated by slip in adjacent equiaxed α grains or colonies, the crystallographic orientation of equiaxed α grains or lamellas containing the incoming slip bands is also reported in figure 13. Prismatic or basal slip activity is likely for these crystallographic orientations. A slip traces analysis confirmed that both basal and prismatic slip bands were able to stimulate twinning in a neighboring grain with a low declination angle.

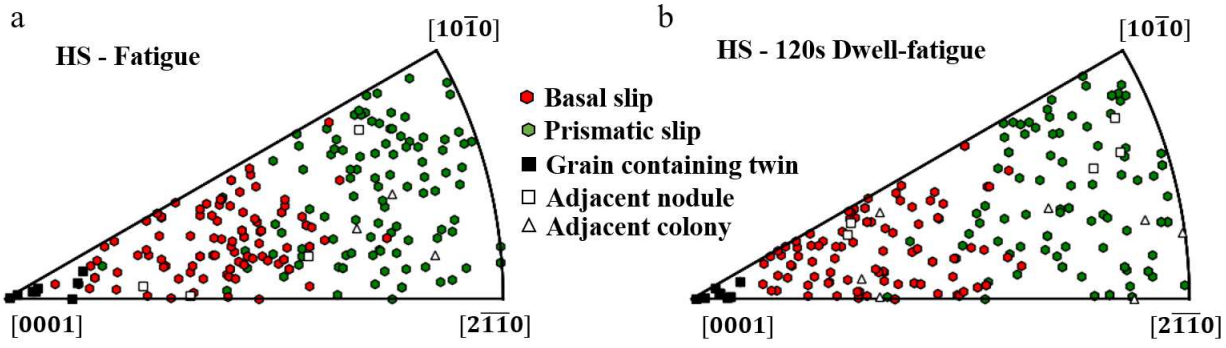

Figure 13: Crystallographic orientation of α grains containing basal slip traces, prismatic slip traces or twins at a cumulated plastic strain of 0.025 for the a) fatigue and b) 120 s dwell-fatigue HS tests. The orientation of α grains and colonies containing the slip bands which have stimulated twinning is also indicated. Orientations are relative to the loading direction.

As previously mentioned, twins were not observed in all α grains with a declination angle lower than 20°. The absence of incoming slip band, which seems mandatory for the occurrence of twinning, or the competition with slip transfer, which is illustrated in figure 11, are the main causes identified. However, the prediction of the occurrence of twinning is still difficult. Prior studies suggested several parameters which can be used to assess its likeliness. In particular, several researchers discussed an effect of the resolved shear stress and a potential applicability of Schmid's law *[52,53]*. The active and inactive twinning variants are plotted in figure 14 as a function of the Schmid factor regardless of the loading condition. Parent α grains exhibit Schmid factors for twinning higher than 0.4. To account for the features of the incoming slip band, two other parameters were considered: the Schmid factor and the *m'* parameter. The Schmid factor indicates the likeliness of a given slip system to be activated in the early deformation stages. As deformation follows patterns which are established at the beginning of loading, it is also an indicator the magnitude of the plastic strain experienced by the grain *[40]*. The *m'* parameter introduced by Luster and Morris *[45]* was used to evaluate the geometric alignment between incoming and outgoing deformation systems. The active and inactive twinning variants are plotted in figure 14 as a function of the Schmid factor of the incoming slip bands and *m'* regardless of the loading condition. Twinning was observed to occur for *m'* values higher than 0.2 and Schmid factor values for the incoming slip system higher than 0.43. Most twins are located in a domain defined by *m'* values higher than 0.85 and Schmid factor values higher than 0.46. However, interactions without twin formation were found for values of *m'* and Schmid factors within this domain.

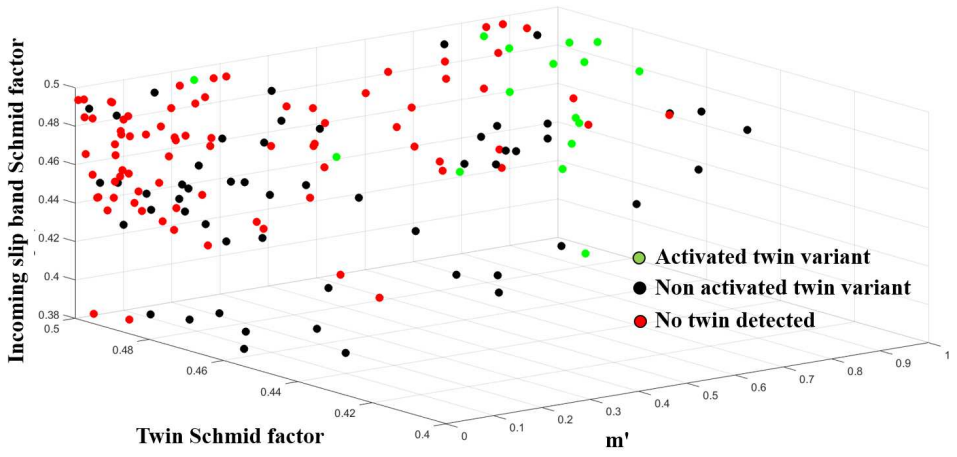

Figure 14 : Active and inactive twinning variants plotted with respect to the Schmid factor of the variant, the Schmid factor of the incoming slip system and the m' values associated with the alignment of both deformation systems for all the interactions between a slip band and the boundary of an α grain with a declination lower than 20° at a cumulated plastic strain of 0.025 for the fatigue and 120 s dwell-fatigue HS tests

4. Discussion

4.1 *Deformation processes under cyclic loadings in Ti-6Al-4V*

A statistically sound investigation of the operating deformation processes was carried out in the present study. While prior works mostly focused on monotonic loadings, cyclic loadings were presently considered. In particular, the influence of the load hold duration was examined. Fatigue and dwell-fatigue are often addressed as different topics, which may lead to a difficult comparison. This work thus allows an improved knowledge of active deformation processes in relation with the crystallographic orientation for such loading conditions, but also revealed numerous possible

interactions between slip bands and grain boundaries, which are key for the understanding of the crack nucleation process. In agreement with the findings of Bridier et al. for strain controlled low cycle fatigue tests [36], basal and prismatic slip were observed to be the dominant slip systems regardless of the loading conditions. The orientation of α grains with basal or prismatic slip traces is in good agreement with prior works on bimodal Ti-6Al-4V under tension and strain controlled fatigue loadings [13,36,47]. Although only these slip modes were detected after a low number of cycles of the LS tests, other deformation modes were active at higher cumulated plastic strains.

<**c+a**> pyramidal slip is usually expected to accommodate **c**-axis deformation in hard grains. It was frequently observed for declination angles up to 30°. The high CRSS value for 1st order <**c+a**> pyramidal slip, which is roughly 1.6 times the CRSS of basal slip [16,54], does not prevent its activation. Thus, the occurrence of <**c+a**> pyramidal slip has to be systematically considered in order to study fatigue and dwell-fatigue. Considering higher declination angles, <**a**> and <**c+a**> pyramidal slip were occasionally observed for very high Schmid factors and moderate basal and prismatic Schmid factors. The associated orientation domain also contains a significant overlap of basal and prismatic slip activities. In addition, the occurrence of grain boundary sliding was detected in the same orientation domain. In agreement with the work of Hémery et al. [50], this process seems stimulated by intragranular prismatic slip.

$\{10\bar{1}2\}\langle 10\bar{1}1\rangle$ twins were occasionally noticed in α grains with a declination angle lower than 20°. As reported in [30], twins were systematically found to result from slip band / grain boundary interactions. In contrast with **<a>** slip, $\{10\bar{1}2\}\langle 10\bar{1}1\rangle$ extension twinning is able to accommodate deformation along the **c**-axis [1]. The understanding of conditions promoting or inhibiting twinning is thus a major concern to improve the performance of titanium alloys. The Schmid factor associated with the incoming slip band was found correlated with the occurrence of twinning. Indeed, twins were noticed for Schmid factor values higher than 0.38 while basal or prismatic slip activity was observed for Schmid factors as low as 0.2. This indicates a high likeliness of such a slip system to be activated in the early deformation stages. As deformation follows patterns which are established at the beginning of loading, it is also a qualitative indicator the magnitude of the plastic strain experienced by the α grain [40]. This is consistent with the findings of Bieler et al. who showed that the deformation history in neighboring grains needs to be considered [55]. The occurrence of twinning is also influenced by the alignment between the incoming and outgoing deformation systems which can be quantified by the *m'* parameter [56–58]. The present study demonstrates that this finding holds for Ti-6Al-4V as well. In addition, Schmid factors of the twinning variants observed were systematically close to 0.5. However, these parameters presently failed at predicting the occurrence of twinning. The complex stress states induced by dislocation pile-ups might have to be considered for a more realistic prediction. Furthermore, twinning could be inhibited owing to the competition with other processes such as slip transfer or boundary sliding. Finally, prior studies suggested an effect of the free surfaces on twinning [59]. Additional EBSD characterization was performed after mechanical sectioning of a 120 s dwell-fatigue HS tested specimen up to 9 % cumulated plastic strain. The crystallographic orientation map shown in figure 15 reveals the subsurface occurrence of twinning.

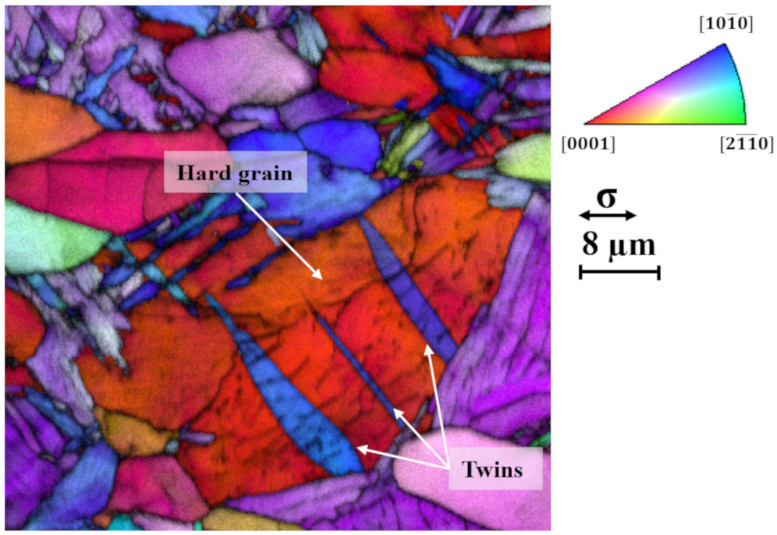

Figure 15: Crystallographic orientation map relative to the loading axis. Twins are observed in a hard grain within the bulk of a 120 s dwell–fatigue HS tested specimen at a plastic strain of 0.09

To sum up, the various deformation processes observed are indicated with respect to the crystallographic orientation in figure 16 based on the 120 s dwell-fatigue HS test. A concurrent operation of **<c+a>** pyramidal slip and twinning was observed for declination angles below 10°. The absence of **<a>** slip in this orientation domain reveals that it only contains hard grains. Beyond 10°, basal slip occurrences were found and a competition between **<c+a>** pyramidal slip, twinning and basal slip was observed up to 20°. **<c+a>** pyramidal slip and basal slip were both noticed between 20° and 30°. The definition of a strict orientation domain for hard grains thus remains a challenging issue. This is a critical concern for i) the identification of microstructural configurations favoring high dwell-debits, and ii) an improved forecast of active deformation processes. The latter is key for interpretation of crystallographic orientations on fracture surfaces, such as obtained using quantitative tilt

fractography, where the identification of active slip systems is difficult to perform on a large number of grains.

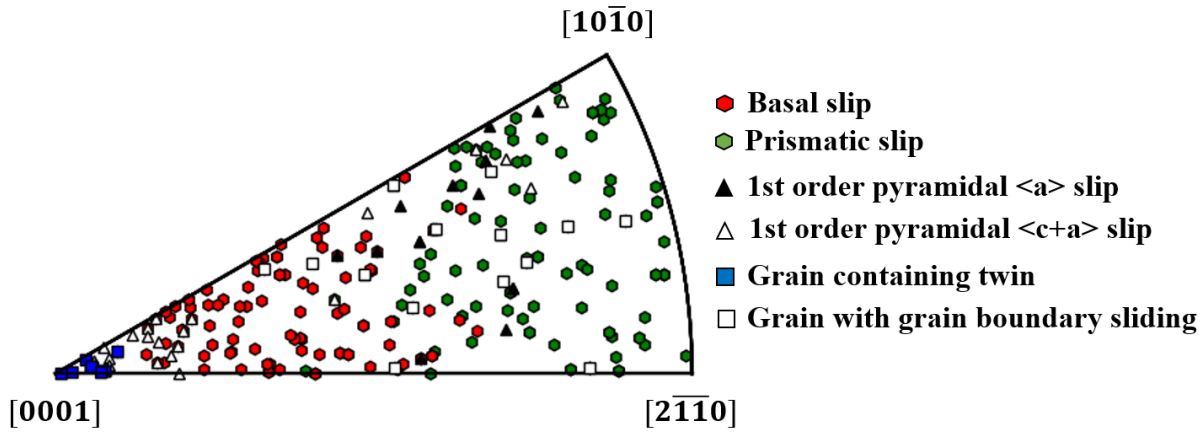

Figure 16 : Crystallographic orientation of α grains showing basal slip, prismatic slip, twins and grain boundary sliding at a plastic strain magnitude of 0.025 for the 120 s dwell-fatigue HS test. Orientations are relative to the loading direction.

4.2 *Effect of loading conditions*

Dwell-sensitivity is usually discussed in terms of a reduction in the number of cycles to failure, but a correlation was found with the evolution of the cumulated plastic strain as a function of the number of cycles [39]. Significant differences in the deformation behavior were found depending on the applied load hold duration. The macroscale behavior revealed a higher plastic strain uptake as the load hold duration is increased. This is consistent with prior results on Ti-6Al-2Sn-4Zr-2Mo and Ti-6Al-2Sn-4Zr-6Mo [37] and illustrates the occurrence of room-temperature creep during load holds [1,60]. This feature is accompanied by significant differences in the deformation behavior at the microscale.

The comparison of 1 cycle of fatigue and 1 cycle of dwell-fatigue with a 120 s load hold showed significantly different slip activities. Although not described above for shortness purposes, similar trends can be extracted from the comparison of the slip activities after 60 fatigue cycles of the LS fatigue test and 65 dwell-fatigue cycles of the LS 120 s dwell-fatigue test. The associated cumulated plastic strains are 10^{-3} and 10^{-2} respectively. The increased load hold duration induced slip activation in α grains less favorably oriented for basal or prismatic slip (i.e. with lower Schmid factors). Regardless of the applied loading waveform, increasing the number of cycles leads to a similar evolution. Cycling promotes the activation of slip systems in α grains less favorably oriented for slip. These observations are in very good agreement with the simulations carried out in prior studies [43,61]. This is an evidence of the occurrence of stress redistribution. The load shedding process occurring from a soft grain onto a hard grain, which has been extensively investigated in prior studies [16–18,20–22,29], is only a specific case of a more general process and has to be considered for soft grains as well. This process explains the observation of prismatic slip activity and basal slip for low declination angles in spite of the low peak stress of LS tests. This is of critical importance to understand the deformation behavior of titanium alloys submitted to cyclic loadings.

Although the abovementioned differences are reduced if similar cumulated plastic strain magnitudes are considered, the detailed analysis of slip activity revealed substantial differences at high cumulated plastic strains depending on the applied load hold duration. While the involved mechanisms remain unchanged in agreement with [37], the present work suggests that their contribution differs substantially. For instance, the number of slip systems involved in the plastic deformation of the

specimen increases with the load hold duration. Basal and prismatic slip activities are concerned by this effect. The number of α grains where soft slip modes are active increases as well. Two consequences stem from these findings. First, strain distributions should be different to reach similar cumulated plastic strain levels. Second, the load is shed on to a restricted number of grains with increasing load hold durations. The increased stress magnitude results in an increase in the likeliness of **<c+a>** pyramidal slip activity in α grains with a low declination angle. This is an experimental evidence of the load shedding phenomenon described in the literature [16,20,21] but also reveals that the intensity of stress redistribution seems influenced by the dwell period, even considering similar cumulated plastic strain magnitudes. These differences in the stress and strain fields will eventually affect the crack initiation and growth processes.

4.3 *The relation with the fatigue and dwell-fatigue performance*

According to prior studies, equiaxed α grains at dwell-fatigue crack nucleation sites exhibit declination angles comprised between 10° and 50° [34]. **<c+a>** pyramidal slip was occasionally found in this study for values up to 30° but only basal slip covers the whole 10° - 50° domain. This suggests a critical role of basal slip in dwell fatigue crack initiation. Similar declination angles were found at fatigue crack initiation sites which suggested a critical role of basal slip in the fatigue crack nucleation process [34,36,38]. The present observations confirm that basal slip operates over this whole declination angle domain under fatigue loadings as well. Basal slip thus seems involved in crack nucleation regardless of the applied load hold duration. Interestingly, α grains with basal slip experience, in average, a higher plastic strain and give rise to more damaging stress redistribution due to the high intrinsic rate sensitivity of this slip mode [62,63].

Facetted crack propagation is often associated with increased growth rates and low fatigue lives. It was found to significantly contribute to the dwell-fatigue life debit noticed in α-β titanium alloys. While striated crack growth is mainly observed in grains with {0001} planes perpendicular to the loading direction, facetted growth was mainly reported in grains with declination angles between 0° and 40° [38,64–66]. In this range, multiple deformation mechanisms such as twinning, **<c+a>** pyramidal slip and basal slip can operate. This result reveals a difficult analysis of deformation mechanisms associated with the cracking process.

Hard grains, where no **<a>** type slip operate, are often considered as critical for the facetted crack growth. The higher number of active slip systems presently noticed in hard grains for high load hold duration reveals that they experience higher stress magnitudes for such load hold durations. Most prior studies considered a similar number of cycles, while this result was shown with similar cumulated plastic strains in the present work. This is important to highlight the influence of the loading history to reach a given accumulated strain. As dwell-fatigue crack initiation and growth is expected to occur at higher cumulated plastic strains than under fatigue loadings, one may infer that this will involve higher strains in soft grains and higher stress in hard grains due to load shedding. Initiated cracks are thus expected to grow through hard grains experiencing higher stress level and a higher number of active slip systems for high load hold durations. As stress and cyclic plasticity drives crack propagation [67], this analysis suggests an explanation for the faster facetted crack growth reported under dwell-fatigue loadings that has been found to significantly contribute to the life debit [38,64–66].

In hard grains, twinning and **<c+a>** pyramidal slip are expected according to the present work. The high stress in such grains, which is believed to play a key role on the dwell sensitivity, might be reduced through acting on the operation of basal slip, **<c+a>** pyramidal slip and twinning. For instance, the ratios of pyramidal CRSS to prismatic CRSS seem relatively insensitive to the aluminum content, which is the main alloying element present in the α phase. Indeed, values around 1.6 are reported for Ti-6Al-4V [68] tested in tension versus 1.9 for commercially pure titanium [69]. In contrast, basal slip and twinning are known to be highly sensitive to the aluminum content of titanium

alloys [70]. To the best of the authors' knowledge, twinning has not been reported to occur at crack initiation sites yet. In addition, facetted crack growth in grains with a declination angle lower than 10° was not reported under dwell-fatigue loading where most of twins were observed [33,34,71]. Then, it is likely to inhibit the early stages of cracking through relaxation of stress concentrations induced by dislocation pile-ups such as involved in the Evans and Bache model [6]. Another beneficial effect of twinning would be the deflection of microcracks propagating across interfaces or grain boundaries as their habit plane is far from the cleavage plane [72]. This analysis illustrates potential pathways to optimize alloys and microstructures in order to temper the dwell effect in titanium alloys.

5 Conclusion

An investigation of deformation processes operating in primary α of cyclically loaded Ti-6Al-4V specimens with a bi-modal microstructure was reported in the present article. A combination of EBSD and slip traces analysis was applied in order to obtain statistically relevant information. Conditions associated with the operation of the different deformation mechanisms were identified and several features previously inferred from crystal plasticity simulations were confirmed by experimental data. In particular, the consequences of the introduction of a load hold at maximum stress on the deformation behavior were analyzed.

- A low peak stress favors the operation of basal slip over prismatic slip. Although basal and prismatic slip were found dominant, the occurrence of **<a>** and **<c+a>** pyramidal slip as well as twinning and grain boundary sliding were evidenced. Various processes resulting from the interactions between slip bands and grain boundaries have to be considered for an accurate prediction of crack initiation and growth.
- All grains with declination angles lower than 10° are hard grains (i.e. deform by **<c+a>** pyramidal slip and occasionally twinning). Between 10° to 20°, basal slip, twinning and **<c+a>** pyramidal slip are concurrently operating. Beyond, twinning disappears but **<c+a>** pyramidal slip still competes with basal slip up to 30°. The present analysis highlights a difficult identification of hard grains which requires the prediction of operating deformation mechanisms.
- The following parameters were found critical for the formation of twins: i. a declination angle for the parent grain lower than 20°, ii. an incident slip band which is not associated with slip transfer or grain boundary sliding, iii. a good alignment between the incoming and outgoing deformation systems and iv. high Schmid factors for the incoming slip and the twinning variant.
- A key role of stress redistribution was experimentally evidenced. Even if the applied stress is insufficient to activate a given slip mode at the first cycle, stress redistribution promoted by the cyclic loading or the load hold eventually enables its operation.
- At a similar number of cycles and different applied load hold durations, the number of active slip systems increased with the cumulated plastic strain and the number of cycles. At a similar cumulated plastic strain, more slip systems are contributing to the global plastic strain for higher load hold durations.
- The number of α grains where basal or prismatic slip occurs increases with the load hold duration, even considering similar cumulated plastic strain levels. The resulting load shedding on to a reduced number of hard grains, which is evidenced through an increased **<c+a>** pyramidal slip activity, may contribute the faster crack growth reported in such grains under dwell fatigue loading.

Acknowledgements

The funding from the Région Poitou-Charentes (Cyril Lavogiez Ph.D. Grant) is gratefully acknowledged.

References

[1] G. Lütjering, J.C. Williams, Titanium, Springer Science & Business Media, 2007.
[2] Z. Song, D. Hoeppner, Dwell time effects on the fatigue behaviour of titanium alloys, Int. J. Fatigue. 10 (1988) 211–218. doi:10.1016/0142-1123(88)90001-1.
[3] M. Bache, A review of dwell sensitive fatigue in titanium alloys: the role of microstructure, texture and operating conditions, Int. J. Fatigue. 25 (2003) 1079–1087. doi:10.1016/S0142-1123(03)00145-2.
[4] W.J. Evans, C.R. Gostelow, The effect of hold time on the fatigue properties of a β-processed titanium alloy, Metall. Trans. A. 10 (1979) 1837–1846. doi:10.1007/BF02811727.
[5] Z. Song, D. Hoeppner, Size effect on the fatigue behaviour of IMI 829 titanium alloy under dwell conditions, Int. J. Fatigue. 11 (1989) 85–90. doi:10.1016/0142-1123(89)90002-9.
[6] W. Evans, M. Bache, Dwell-sensitive fatigue under biaxial loads in the near-alpha titanium alloy IMI685, Int. J. Fatigue. 16 (1994) 443–452. doi:10.1016/0142-1123(94)90194-5.
[7] M.R. Bache, M. Cope, H.M. Davies, W.J. Evans, G. Harrison, Dwell sensitive fatigue in a near alpha titanium alloy at ambient temperature, Int. J. Fatigue. 19 (1997) 83–88. doi:10.1016/S0142-1123(97)00020-0.
[8] D.L. Davidson, D. Eylon, Titanium alloy fatigue fracture facet investigation by selected area electron channeling, Metall. Trans. A. 11 (1980) 837–843. doi:10.1007/BF02661213.
[9] M.R. Bache, W.J. Evans, H.M. Davies, Electron back scattered diffraction (EBSD) analysis of quasi-cleavage and hydrogen induced fractures under cyclic and dwell loading in titanium alloys, (n.d.) 8.
[10] H. Conrad, Effect of interstitial solutes on the strength and ductility of titanium, Prog. Mater. Sci. 26 (1981) 123–403. doi:10.1016/0079-6425(81)90001-3.
[11] I.P. Jones, W.B. Hutchinson, Stress-state dependence of slip in Titanium-6Al-4V and other H.C.P. metals, Acta Metall. 29 (1981) 951–968. doi:10.1016/0001-6160(81)90049-3.
[12] J.C. Williams, R.G. Baggerly, N.E. Paton, Deformation behavior of HCP Ti-Al alloy single crystals, Metall. Mater. Trans. A. (n.d.) 14.
[13] F. Bridier, P. Villechaise, J. Mendez, Analysis of the different slip systems activated by tension in a α/β titanium alloy in relation with local crystallographic orientation, Acta Mater. 53 (2005) 555–567. doi:10.1016/j.actamat.2004.09.040.
[14] J.D. Eshelby, F.C. Frank, F.R.N. Nabarro, XLI. The equilibrium of linear arrays of dislocations., Lond. Edinb. Dublin Philos. Mag. J. Sci. 42 (1951) 351–364. doi:10.1080/14786445108561060.
[15] Y. Guo, T.B. Britton, A.J. Wilkinson, Slip band–grain boundary interactions in commercial-purity titanium, Acta Mater. 76 (2014) 1–12. doi:10.1016/j.actamat.2014.05.015.
[16] V. Hasija, S. Ghosh, M.J. Mills, D.S. Joseph, Deformation and creep modeling in polycrystalline Ti–6Al alloys, Acta Mater. 51 (2003) 4533–4549. doi:10.1016/S1359-6454(03)00289-1.
[17] G. Venkatramani, S. Ghosh, M. Mills, A size-dependent crystal plasticity finite-element model for creep and load shedding in polycrystalline titanium alloys, Acta Mater. 55 (2007) 3971–3986. doi:10.1016/j.actamat.2007.03.017.
[18] G. Venkataramani, K. Kirane, S. Ghosh, Microstructural parameters affecting creep induced load shedding in Ti-6242 by a size dependent crystal plasticity FE model, Int. J. Plast. 24 (2008) 428–454. doi:10.1016/j.ijplas.2007.05.001.
[19] S. Ghosh, P. Chakraborty, Microstructure and load sensitive fatigue crack nucleation in Ti-6242 using accelerated crystal plasticity FEM simulations, Int. J. Fatigue. 48 (2013) 231–246. doi:10.1016/j.ijfatigue.2012.10.022.
[20] F.P.E. Dunne, D. Rugg, A. Walker, Lengthscale-dependent, elastically anisotropic, physically-based hcp crystal plasticity: Application to cold-dwell fatigue in Ti alloys, Int. J. Plast. 23 (2007) 1061–1083. doi:10.1016/j.ijplas.2006.10.013.

[21] F.P.E. Dunne, A. Walker, D. Rugg, A systematic study of hcp crystal orientation and morphology effects in polycrystal deformation and fatigue, Proc. R. Soc. Math. Phys. Eng. Sci. 463 (2007) 1467–1489. doi:10.1098/rspa.2007.1833.
[22] Z. Zheng, D.S. Balint, F.P.E. Dunne, Discrete dislocation and crystal plasticity analyses of load shedding in polycrystalline titanium alloys, Int. J. Plast. 87 (2016) 15–31. doi:10.1016/j.ijplas.2016.08.009.
[23] S. Waheed, Z. Zheng, D.S. Balint, F.P.E. Dunne, Microstructural effects on strain rate and dwell sensitivity in dual-phase titanium alloys, Acta Mater. 162 (2019) 136–148. doi:10.1016/j.actamat.2018.09.035.
[24] Z. Zhang, M.A. Cuddihy, F.P.E. Dunne, On rate-dependent polycrystal deformation: the temperature sensitivity of cold dwell fatigue, Proc. R. Soc. Math. Phys. Eng. Sci. 471 (2015) 20150214. doi:10.1098/rspa.2015.0214.
[25] F.P.E. Dunne, D. Rugg, On the mechanisms of fatigue facet nucleation in titanium alloys, Fatigue Fract. Eng. Mater. Struct. 31 (2008) 949–958. doi:10.1111/j.1460-2695.2008.01284.x.
[26] M.A. Cuddihy, A. Stapleton, S. Williams, F.P.E. Dunne, On cold dwell facet fatigue in titanium alloy aero-engine components, Int. J. Fatigue. 97 (2017) 177–189. doi:10.1016/j.ijfatigue.2016.11.034.
[27] K. Kirane, S. Ghosh, A cold dwell fatigue crack nucleation criterion for polycrystalline Ti-6242 using grain-level crystal plasticity FE Model, Int. J. Fatigue. 30 (2008) 2127–2139. doi:10.1016/j.ijfatigue.2008.05.026.
[28] M. Anahid, M.K. Samal, S. Ghosh, Dwell fatigue crack nucleation model based on crystal plasticity finite element simulations of polycrystalline titanium alloys, J. Mech. Phys. Solids. 59 (2011) 2157–2176. doi:10.1016/j.jmps.2011.05.003.
[29] D. Ozturk, A.L. Pilchak, S. Ghosh, Experimentally validated dwell and cyclic fatigue crack nucleation model for α–titanium alloys, Scr. Mater. 127 (2017) 15–18. doi:10.1016/j.scriptamat.2016.08.031.
[30] C. Lavogiez, S. Hémery, P. Villechaise, Concurrent operation of ⟨c + a⟩ slip and twinning under cyclic loading of Ti-6Al-4V, Scr. Mater. 157 (2018) 30–33. doi:10.1016/j.scriptamat.2018.07.033.
[31] V. Sinha, M.J. Mills, J.C. Williams, J.E. Spowart, Observations on the faceted initiation site in the dwell-fatigue tested ti-6242 alloy: Crystallographic orientation and size effects, Metall. Mater. Trans. A. 37 (2006) 1507–1518. doi:10.1007/s11661-006-0095-x.
[32] V. Sinha, M.J. Mills, J.C. Williams, Determination of crystallographic orientation of dwell-fatigue fracture facets in Ti-6242 alloy, J. Mater. Sci. 42 (2007) 8334–8341. doi:10.1007/s10853-006-0252-z.
[33] E. Uta, N. Gey, P. Bocher, M. Humbert, J. Gilgert, Texture heterogeneities in α_p/α_s titanium forging analysed by EBSD-Relation to fatigue crack propagation, J. Microsc. 233 (2009) 451–459. doi:10.1111/j.1365-2818.2009.03141.x.
[34] A.L. Pilchak, J.C. Williams, Observations of Facet Formation in Near-α Titanium and Comments on the Role of Hydrogen, Metall. Mater. Trans. A. 42 (2011) 1000–1027. doi:10.1007/s11661-010-0507-9.
[35] P.O. Tympel, T.C. Lindley, E.A. Saunders, M. Dixon, D. Dye, Macrozones and dwell fatigue crack initiation in Ti-6Al-4V, in: V. Venkatesh, A.L. Pilchak, J.E. Allison, S. Ankem, R. Boyer, J. Christodoulou, H.L. Fraser, M.A. Imam, Y. Kosaka, H.J. Rack, A. Chatterjee, A. Woodfield (Eds.), Proc. 13th World Conf. Titan., John Wiley & Sons, Inc., Hoboken, NJ, USA, 2016: pp. 985–991. doi:10.1002/9781119296126.ch168.
[36] F. Bridier, P. Villechaise, J. Mendez, Slip and fatigue crack formation processes in an α/β titanium alloy in relation to crystallographic texture on different scales, Acta Mater. 56 (2008) 3951–3962. doi:10.1016/j.actamat.2008.04.036.
[37] S. Hémery, P. Villechaise, Comparison of slip system activation in Ti-6Al-2Sn-4Zr-2Mo and Ti-6Al-2Sn-4Zr-6Mo under tensile, fatigue and dwell-fatigue loadings, Mater. Sci. Eng. A. 697 (2017) 177–183. doi:10.1016/j.msea.2017.05.021.
[38] I. Bantounas, D. Dye, T.C. Lindley, The effect of grain orientation on fracture morphology during high-cycle fatigue of Ti–6Al–4V, Acta Mater. 57 (2009) 3584–3595. doi:10.1016/j.actamat.2009.04.018.

[39] J. Qiu, Y. Ma, J. Lei, Y. Liu, A. Huang, D. Rugg, R. Yang, A Comparative Study on Dwell Fatigue of Ti-6Al-2Sn-4Zr-xMo (x = 2 to 6) Alloys on a Microstructure-Normalized Basis, Metall. Mater. Trans. A. 45 (2014) 6075–6087. doi:10.1007/s11661-014-2541-5.
[40] P.D. Littlewood, A.J. Wilkinson, Local deformation patterns in Ti–6Al–4V under tensile, fatigue and dwell fatigue loading, Int. J. Fatigue. 43 (2012) 111–119. doi:10.1016/j.ijfatigue.2012.03.001.
[41] D. Lunt, J.Q. da Fonseca, D. Rugg, M. Preuss, Microscopic strain localisation in Ti-6Al-4V during uniaxial tensile loading, Mater. Sci. Eng. A. 680 (2017) 444–453. doi:10.1016/j.msea.2016.10.099.
[42] D. Lunt, T. Busolo, X. Xu, J. Quinta da Fonseca, M. Preuss, Effect of nanoscale α 2 precipitation on strain localisation in a two-phase Ti-alloy, Acta Mater. 129 (2017) 72–82. doi:10.1016/j.actamat.2017.02.068.
[43] F. Bridier, D.L. McDowell, P. Villechaise, J. Mendez, Crystal plasticity modeling of slip activity in Ti–6Al–4V under high cycle fatigue loading, Int. J. Plast. 25 (2009) 1066–1082. doi:10.1016/j.ijplas.2008.08.004.
[44] S. Hémery, A. Nait-Ali, P. Villechaise, Combination of in-situ SEM tensile test and FFT-based crystal elasticity simulations of Ti-6Al-4V for an improved description of the onset of plastic slip, Mech. Mater. 109 (2017) 1–10. doi:10.1016/j.mechmat.2017.03.013.
[45] J. Luster, M.A. Morris, Compatibility of deformation in two-phase Ti-Al alloys: Dependence on microstructure and orientation relationships, Metall. Mater. Trans. A. 26 (1995) 1745–1756. doi:10.1007/BF02670762.
[46] S. Hémery, V.T. Dang, L. Signor, P. Villechaise, Influence of Microtexture on Early Plastic Slip Activity in Ti-6Al-4V Polycrystals, Metall. Mater. Trans. A. (2018) 1–9. doi:10.1007/s11661-018-4569-4.
[47] S. Hémery, P. Villechaise, On the influence of ageing on the onset of plastic slip in Ti-6Al-4V at room temperature: Insight on dwell fatigue behavior, Scr. Mater. 130 (2017) 157–160. doi:10.1016/j.scriptamat.2016.11.042.
[48] S. Hémery, P. Villechaise, Investigation of Size Effects in Slip Strength of Titanium Alloys: α Nodule Size Dependence of the Critical Resolved Shear Stress, Metall. Mater. Trans. A. (2018) 1–4. doi:10.1007/s11661-018-4678-0.
[49] V. Sinha, M.J. Mills, J.C. Williams, Understanding the contributions of normal-fatigue and static loading to the dwell fatigue in a near-alpha titanium alloy, Metall. Mater. Trans. A. 35 (2004) 3141–3148. doi:10.1007/s11661-004-0058-z.
[50] S. Hémery, C. Tromas, P. Villechaise, Slip-stimulated grain boundary sliding in Ti-6Al-4 V at room temperature, Materialia. 5 (2019) 100189. doi:10.1016/j.mtla.2018.100189.
[51] M.P. Echlin, J.C. Stinville, V.M. Miller, W.C. Lenthe, T.M. Pollock, Incipient slip and long range plastic strain localization in microtextured Ti-6Al-4V titanium, Acta Mater. 114 (2016) 164–175. doi:10.1016/j.actamat.2016.04.057.
[52] L. Xiao, Twinning behavior in the Ti–5at.% Al single crystals during cyclic loading along [0001], Mater. Sci. Eng. A. 394 (2005) 168–175. doi:10.1016/j.msea.2004.11.039.
[53] F. Coghe, W. Tirry, L. Rabet, D. Schryvers, P. Van Houtte, Importance of twinning in static and dynamic compression of a Ti–6Al–4V titanium alloy with an equiaxed microstructure, Mater. Sci. Eng. A. 537 (2012) 1–10. doi:10.1016/j.msea.2011.12.047.
[54] M. Kasemer, M.P. Echlin, J.C. Stinville, T.M. Pollock, P. Dawson, On slip initiation in equiaxed α/β Ti-6Al-4V, Acta Mater. 136 (2017) 288–302. doi:10.1016/j.actamat.2017.06.059.
[55] T.R. Bieler, L. Wang, A.J. Beaudoin, P. Kenesei, U. Lienert, In Situ Characterization of Twin Nucleation in Pure Ti Using 3D-XRD, Metall. Mater. Trans. A. 45 (2013) 109–122. doi:10.1007/s11661-013-2082-3.
[56] L. Wang, Y. Yang, P. Eisenlohr, T.R. Bieler, M.A. Crimp, D.E. Mason, Twin Nucleation by Slip Transfer across Grain Boundaries in Commercial Purity Titanium, Metall. Mater. Trans. A. 41 (2010) 421–430. doi:10.1007/s11661-009-0097-6.
[57] G. Liu, R. Xin, X. Shu, C. Wang, Q. Liu, The mechanism of twinning activation and variant selection in magnesium alloys dominated by slip deformation, J. Alloys Compd. 687 (2016) 352–359. doi:10.1016/j.jallcom.2016.06.136.

[58] D. Guan, B. Wynne, J. Gao, Y. Huang, W.M. Rainforth, Basal slip mediated tension twin variant selection in magnesium WE43 alloy, Acta Mater. 170 (2019) 1–14. doi:10.1016/j.actamat.2019.03.018.
[59] C.D. Barrett, H. El Kadiri, M.A. Tschopp, Breakdown of the Schmid law in homogeneous and heterogeneous nucleation events of slip and twinning in magnesium, J. Mech. Phys. Solids. 60 (2012) 2084–2099. doi:10.1016/j.jmps.2012.06.015.
[60] T. Neeraj, D.-H. Hou, G.S. Daehn, M.J. Mills, Phenomenological and microstructural analysis of room temperature creep in titanium alloys, Acta Mater. 48 (2000) 1225–1238. doi:10.1016/S1359-6454(99)00426-7.
[61] M.H. Pourian, F. Bridier, P. Pilvin, P. Bocher, Prediction of crack initiation sites in alpha Ti-alloys microstructures under dwell-fatigue using Cellular Automaton simulation method, Int. J. Fatigue. 85 (2016) 85–97. doi:10.1016/j.ijfatigue.2015.12.010.
[62] S. Hémery, P. Villechaise, In situ EBSD investigation of deformation processes and strain partitioning in bi-modal Ti-6Al-4V using lattice rotations, Acta Mater. 171 (2019) 261–274. doi:10.1016/j.actamat.2019.04.033.
[63] Phase morphology, variants and crystallography of alloy microstructures in cold dwell fatigue, Int. J. Fatigue. 113 (2018) 324–334. doi:10.1016/j.ijfatigue.2018.03.030.
[64] I. Bantounas, D. Dye, T.C. Lindley, The role of microtexture on the faceted fracture morphology in Ti–6Al–4V subjected to high-cycle fatigue, Acta Mater. 58 (2010) 3908–3918. doi:10.1016/j.actamat.2010.03.036.
[65] A.L. Pilchak, Fatigue crack growth rates in alpha titanium: Faceted vs. striation growth, Scr. Mater. 68 (2013) 277–280. doi:10.1016/j.scriptamat.2012.10.041.
[66] A.L. Pilchak, A simple model to account for the role of microtexture on fatigue and dwell fatigue lifetimes of titanium alloys, Scr. Mater. 74 (2014) 68–71. doi:10.1016/j.scriptamat.2013.10.024.
[67] U. Krupp, Fatigue Crack Propagation in Metals and Alloys: Microstructural Aspects and Modelling Concepts, 1 edition, Wiley-VCH, Weinheim, 2007.
[68] P.R. Dawson, D.E. Boyce, J.-S. Park, E. Wielewski, M.P. Miller, Determining the strengths of HCP slip systems using harmonic analyses of lattice strain distributions, Acta Mater. 144 (2018) 92–106. doi:10.1016/j.actamat.2017.10.032.
[69] B. Barkia, V. Doquet, J.P. Couzinié, I. Guillot, E. Héripré, In situ monitoring of the deformation mechanisms in titanium with different oxygen contents, Mater. Sci. Eng. A. 636 (2015) 91–102. doi:10.1016/j.msea.2015.03.044.
[70] A. Fitzner, D.G.L. Prakash, J.Q. da Fonseca, M. Thomas, S.-Y. Zhang, J. Kelleher, P. Manuel, M. Preuss, The effect of aluminium on twinning in binary alpha-titanium, Acta Mater. 103 (2016) 341–351. doi:10.1016/j.actamat.2015.09.048.
[71] P.O. Tympel, T.C. Lindley, E.A. Saunders, M. Dixon, D. Dye, Influence of complex LCF and dwell load regimes on fatigue of Ti–6Al–4V, Acta Mater. 103 (2016) 77–88. doi:10.1016/j.actamat.2015.09.014.
[72] Y. Ma, Q. Xue, H. Wang, S. Huang, J. Qiu, X. Feng, J. Lei, R. Yang, Deformation twinning in fatigue crack tip plastic zone of Ti-6Al-4V alloy with Widmanstatten microstructure, Mater. Charact. 132 (2017) 338–347. doi:10.1016/j.matchar.2017.08.029.